

## APPLYING OF THE NEW GENERATION PLASTIC ADDITIVES TO THE KITCHEN APPLIANCES: INVESTIGATION OF STRUCTURAL AND THERMOSTATIC PROPERTIES OF ORGANOMETALLIC MN (II) AND CU (II) STREAT- BORATE COMPLEXES

İlkan KAVLAK

Br Dizayn Mobilya İnşaat ve Isıtma ve Soğutma Sistemleri A.Ş., Industrial Design Centre, Eskişehir Industrial Area, Turkey.

### ABSTRACT

In this study, two new organometallic stearate complexes are described in  $Mn(C_{18}H_{35}O_2)_2 \cdot (B_4O_7)$  (1) and  $Cu(C_{18}H_{35}O_2)_2 \cdot (B_4O_7)$  (2) have been synthesized as plastic additive materials. Thermostatic behaviors of the complexes have been analyzed with described methodology at the ISO 182-2 standard. Additionally, the structural properties of the synthesized complexes were investigated by elemental analysis, powder XRD, and vibrational (FT-IR and Raman) spectroscopic techniques.

The Thermostatic analyses show that synthesized complexes act as a strong HCl scavenger during plastic decomposition. If the plastic dough is composed of strong HCl scavenger agents. The heating resistance capacity will be increased. According to the thermostatic analysis results, the synthesized complexes have been added to the PVC rough as plastic additives. Then, Plasticized complexes were injected into the plastic mold. The obtained plastic materials have been used in domestic built-in hobs as thermal insulator gaskets at the burner pools. The thermally insulated behaviors of the new generation plastic additives have been observed via Elimko 32T channel probes digital thermometers and analyzed with described methodology at the TS EN 30-1-1+A3:2014 standard.

The results are shown that both complexes behaved as thermal barriers between surface of built-in hobs and burners. The thermal decay of the plastic doughs is following  $1 > 2$ .

**Keywords:** PVC, plastic additives, heat-barrier, organometallic complex, EN ISI 182-2, Dehydrochlorination, HCl scavengers, EN 30-1-1+A3:2014, built-in hobs.

### 1. INTRODUCTION

Plastic is an important raw material for products or product groups that make our daily life easier in a wide area, from household appliances to the production of automotive spare parts, from the door and window joinery systems to packaging materials. Since plastic is an easily produced and recyclable material are needed for insulator, heat barrier, mold material, prototype material as a product group, or the production of electronic device appliances and home appliances as products. It is also widely used in the white goods industry as a plastic raw material. It is used as sound insulation materials on the engine covers and engine walls for aspirators or hoods. Similarly, the heat barrier, thermal insulator, liquid sealing gaskets, gas sealing gaskets, and gas control systems are used for built-in hobs and ovens. The plastic additive materials which, are included in the plastic dough, contribute to applying plastic in such a wide range as a raw material. In this study, polyvinylchloride (PVC) was used as plastic raw material, and Mn(II) or Cu(II) metal complexes of stearate and borax molecules were synthesized with an aim of thermal plastic additives applied as a heat barrier in built-in hobs production. The synthesized plastic additives will trap the hydrochloric acid (HCl) gas ions released during the thermal degradation of polyvinyl chloride (PVC) into their molecular structures, thus allowing the thermal degradation rate of PVC to be delayed and prevented [1]. Many studies examining the effects of Stearic Acid, borax and barbiturate molecules and their metal complexes on the thermal stability of PVC are available in the literature [2, 3] [4]. [1, 5-9]. Within this context, the borax and stearate-based metal (II) complexes were synthesized as powder. These complexes were investigated by elemental analysis, powder XRD diffraction techniques, XRF spectroscopy, thermoanalytic analyses techniques (TG, DTG, DTA). Additionally, the vibrational properties of the complexes were studied by FT-IR and Raman spectral techniques. Furthermore, the new generation PVC dough were prepared with synthesized complexes in order to reach out thermal stabilization effect on PVC degradation. The new generation PVC doughs

\*Corresponding Author: [ilkankavlak@brdizayn.com.tr](mailto:ilkankavlak@brdizayn.com.tr)

were plasticized via gelation methods. Hence, the new plastic materials were manufactured. Dehydrochlorination test was performed which is described methods in EN ISO 182-2 standards. The plastic materials were shaped as gasket. Then the plastic materials have applied as surrounded burner pools between built-in hobs surfaces. Thermal barrier properties have been controlled via 32 channel thermometers with their thermocouple by Elimko 32T digital thermometer device. The test results were shown that synthesized complexes were behaved as thermal stabilizer in the PVC dough and the plastic materials behaves thermal barrier between built in hob surface and burners.

## 2. MATERIALS AND METHODS

The tests and analyses performed on the new generation plastic additives obtained from stearate and borate-based Mn(II) and Cu(II) metal complexes, which are intended to be used as a heat barrier in built-in hobs and ovens, are listed in Table 1.

Table 1. Test and Analyses for new generation plastic additives

The molecular formula of New Generation Plastic Additives	Analyses Methods						Thermal Stability Test Ref: ISO EN 182-2	The test of thermal barrier applying Surface Temperature (°C) Ref: EN 30-2-2+1
	Elemental Analyses	XRD	XRF	FT- IR	Raman	TG-DTG- DTA		
Mn(C <sub>18</sub> H <sub>36</sub> O <sub>2</sub> ) <sub>2</sub> ·(B <sub>4</sub> O <sub>7</sub> )·2H <sub>2</sub> O	■	■	■	■	■	■	■/ 65	■/96-142
Cu(C <sub>18</sub> H <sub>35</sub> O <sub>2</sub> ) <sub>2</sub> ·(B <sub>4</sub> O <sub>7</sub> ) H <sub>2</sub> O	■	■	■	■	■	■	■/ 57	■/ 108-142

### 2.1. Materials

All materials, copper (II) chloride dihydrate (CuCl<sub>2</sub>·2H<sub>2</sub>O, 99%), Manganese(II) chloride tetrahydrate (MnCl<sub>2</sub>·4H<sub>2</sub>O, 99%) Sodium stearate (CH<sub>3</sub>(CH<sub>2</sub>)<sub>16</sub>COONa, 97%) and sodium tetraborate anhydrous (Na<sub>2</sub>B<sub>4</sub>O<sub>7</sub>, 99.5%) were used as received from commercial sources.

### 2.2. Syntheses of the complexes

2 mmol sodium stearate was solved in the ethanol and stirred for 2 hours. To provide the best solvent, the solution is warmed to 50 °C and slightly added the ethanol due to evaporation. 1 mmol of metal salts (CuCl<sub>2</sub>·2H<sub>2</sub>O)(aq) or (MnCl<sub>2</sub>·4H<sub>2</sub>O)(aq) was added dropwise to the solution. The solutions are stirred for 1 hour. On the other hand, Sodium tetra borate is solved in warm water (100 °C). Sodium tetra borate is added dropwise to the solution. The mixture was stirred for 14 hours. After stirring for 14 hours, the complexes collapsed. Then, the solutions were filtered and dried at room temperatures. Finally, The colors of the obtained complexes for Mn(II) and Cu(II) are brown and blue, respectively. The freshly prepared complexes were analyzed for C, H and N and the results are given in Table 2. Elemental analyses are in good agreement with the calculated values.

Table 2. Molecular formula for complexes

Complex	Molecular Formula	M <sub>A</sub> (g/mol)		% C	% H	% N
1	Mn(C <sub>18</sub> H <sub>36</sub> O <sub>2</sub> ) <sub>2</sub> ·(B <sub>4</sub> O <sub>7</sub> )·2H <sub>2</sub> O	815,50	Experimental	54,8	9,22	-
			Theoretical	54,38	9,13	-
2	Cu(C <sub>18</sub> H <sub>35</sub> O <sub>2</sub> ) <sub>2</sub> ·(B <sub>4</sub> O <sub>7</sub> ) H <sub>2</sub> O	805,49	Experimental	55,73	9,35	-
			Theoretical	53,80	9,03	-

Similarly, determined closed formulas of the complexes by elemental analysis methods were supported by thermogravimetric analysis. For **1** complex, according to the DT-DSC thermal degradation curve of the complexes, it shows a stable structure up to 306 °C (Figure 1).

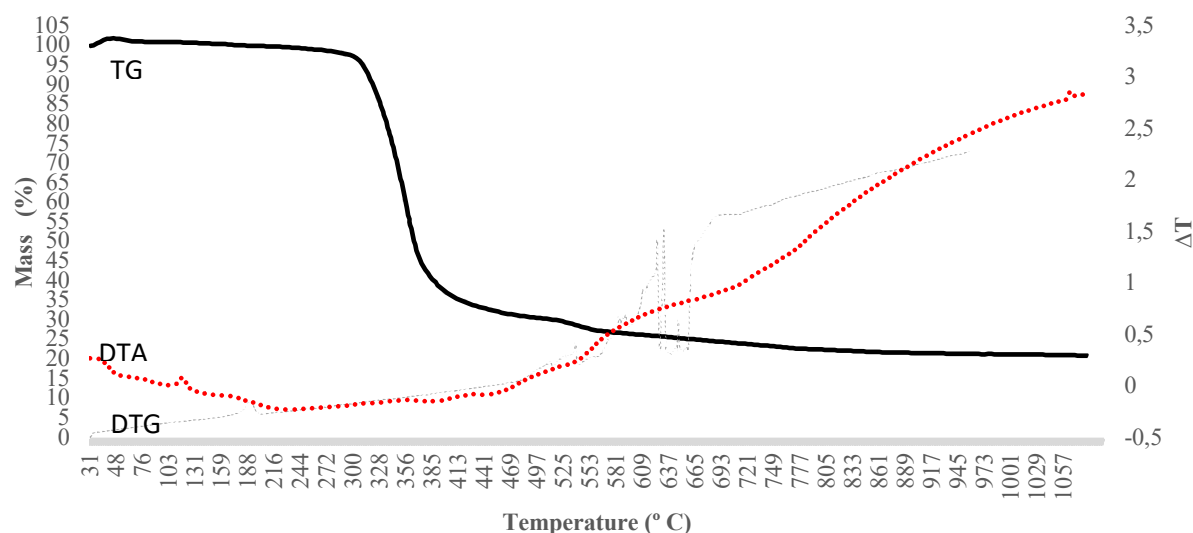


Figure 1. The TG, DTG, and DTA curves of the complex 1

The **1** complex decomposed in 3 stages in the temperature range of 30-1059 °C as seen Table 3. It is seen that 2 moles of H<sub>2</sub>O molecules, corresponding to 4.5% of the total mass, are separated from the complex in the temperature range of 30-306 °C. 2 moles of stearic acid were removed from the complex in the temperature range of 306-411 °C. It is separated into two different forms as B<sub>2</sub>O<sub>4</sub> and B<sub>2</sub>O<sub>3</sub> in the temperature range of 411-567 °C from the complex. B<sub>2</sub>O<sub>4</sub> left the structure while B<sub>2</sub>O<sub>3</sub> remained unchanged. Finally, the curve stabilized in the temperature range of 567-1059 °C and MnO and B<sub>2</sub>O<sub>3</sub> materials, corresponding to 21% of the total mass, remained.

Table 3. Thermoanalytical Data (TG, DTG, DTA) for the complex 1

Temperature Range	Compounds	Removed Group	Solid decomposition Compounds Stage product (MA)	Removed Group (MA)	Mass loan (%)	
					Found (%)	Calculated (%)
30-306 °C	Mn(C <sub>18</sub> H <sub>36</sub> O <sub>2</sub> ) <sub>2</sub> B <sub>4</sub> O <sub>7</sub> ·2H <sub>2</sub> O	2H <sub>2</sub> O	815,5	36,02	4,50%	4,51%
306-411 °C	Mn(C <sub>18</sub> H <sub>36</sub> O <sub>2</sub> ) <sub>2</sub> B <sub>4</sub> O <sub>7</sub>	(C <sub>18</sub> H <sub>36</sub> O <sub>2</sub> ) <sub>2</sub>	779,13	568,54	66,54%	69,71%
411-567 °C	Mn·B <sub>4</sub> O <sub>7</sub>	B <sub>2</sub> O <sub>4</sub>	210,94	86	8%	10,54%
567-1059 °C		CdO+B <sub>2</sub> O <sub>3</sub> +CO <sub>2</sub>	199,5	-	21%	24,46%

For **2** Complex, the thermal degradation curve of the complex is given in Figure 2. Here, it has been determined that the Complex degrades in 3 stages in the range of 30-1068 °C. The thermoanalytic decomposition steps of the complex and the percentage of separated material are listed in Table 4. It is seen that the complex is stable up to a temperature value of 212 °C. After this temperature value, 1 mol of H<sub>2</sub>O molecule is separated from the complex which corresponds to 2.23% of the total mass.

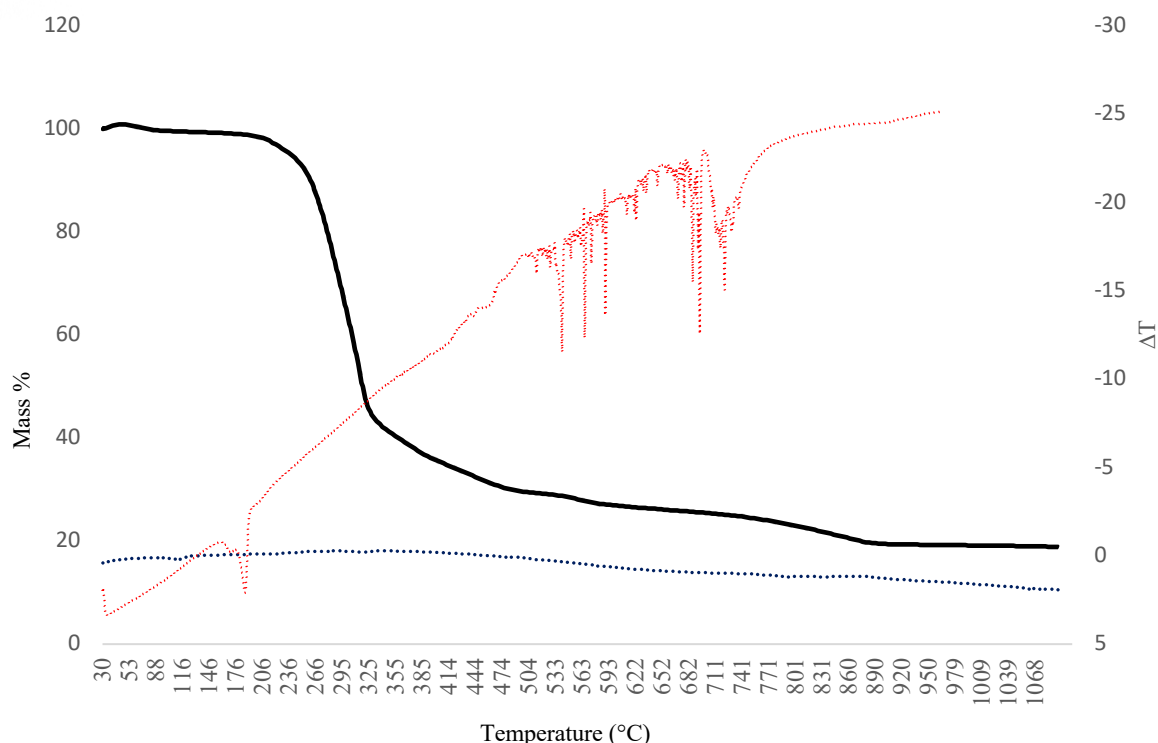


Figure 2. The TG, DTG, and DTA curves of the complex 2

In the temperature range of 212-419 °C, 2 moles of stearic acid were removed from the structure. Borate was separated into two different forms B<sub>2</sub>O<sub>4</sub> and B<sub>2</sub>O<sub>3</sub> in the temperature range of 419-852 °C, and B<sub>2</sub>O<sub>4</sub> was separated from the structure in this temperature range. In the temperature range of 852-1068 °C, it was determined that CuO and B<sub>2</sub>O<sub>3</sub>, which constitute 19% of the initial mass, remained.

Table 4. Thermoanalytical Data (TG, DTG, DTA) for the complex 2

Temperature Range	Compounds	Removed Group	Solid decomposition Compounds Stage product (MA)	Removed Group (MA)	Mass loan (%)	
					Found (%)	Calculated (%)
30-306 °C	Cu(C <sub>18</sub> H <sub>36</sub> O <sub>2</sub> ) <sub>2</sub> B <sub>4</sub> O <sub>7</sub> ·2H <sub>2</sub> O	H <sub>2</sub> O	805,49	18,01	2%	2,23%
306-411 °C	Cu(C <sub>18</sub> H <sub>36</sub> O <sub>2</sub> ) <sub>2</sub> B <sub>4</sub> O <sub>7</sub>	(C <sub>18</sub> H <sub>36</sub> O <sub>2</sub> ) <sub>2</sub>	787,48	568,54	68%	70%
411-567 °C	Cu·B <sub>4</sub> O <sub>7</sub>	B <sub>2</sub> O <sub>4</sub>	218,79	86	9%	10,67%
567-1059 °C	-	CuO+B <sub>2</sub> O <sub>3</sub> +CO <sub>2</sub>	199,5	-	19%	18,51%

### 2.3. Plasticizing

The plastic dough is blended with k=74 hardness PVC, 5% by mass, CaCO<sub>3</sub> by mass, 5% by mass of chlorinated polyethylene, and 5% by mass of plastic additive materials. Mass values in the plastic recipe are not a rule, they are the values at which the best fluid plastic is obtained after blending. The best flow rates were obtained with these values for the plastic blend prepared by the gelling method. After preparing the plastic blend, the mixtures were stirred mechanical mixer. When the blend were mixed with a mechanical mixer, acetone was added drop by drop. The obtained liquid mixtures are dropped plastic mold and pressed after the molds are baked in the oven at 170 °C for 15 minutes. After baking, the plastic molds are dropped in the cold water. Finally, plastic materials are obtained.

### 2.4. Physical measurements

The complexes obtained were performed elemental analyses. Elemental analyses were carried out on LECO, CHNS-932 analyzer for C, H, and N at the Middle East Technical University Central Laboratory.

FT-IR and Raman spectra of the complexes were recorded in the region of 4000–250  $\text{cm}^{-1}$  via Perkin-Elmer FT-IR 100 spectrometer at a resolution of 4  $\text{cm}^{-1}$  and Bruker Senterra Dispersive Raman Microscope using the 785 nm line of a 3B diode laser, respectively. Perkin Elmer Diamond TG/DTA thermal analyzer was used to record simultaneous TG, DTG, and DTA curves in the static air atmosphere at a heating rate of 10  $\text{K min}^{-1}$  in the temperature range of 30–700  $^{\circ}\text{C}$  using platinum crucibles at the Eskişehir Osmangazi University Central Laboratory (ARUM). The XRD patterns of the powder products were obtained on a Rigaku Rint 2200 diffractometer using  $\text{Cu-K}\alpha$  radiation. Then, the molecular structures were obtained by powder XRD diffractometers. Meanwhile, the PXRD data were solved via the Rietveld analysis program as Match 3.0 [10]. XRF data of the complexes were obtained in the Rikagu ZSX PRIMUS device in Eskişehir Technical University Physics Department. The standards used;  $\text{Na}_2\text{O}$ ,  $\text{SiO}_2$ ,  $\text{Fe}_2\text{O}_3$ ,  $\text{NiO}$ ,  $\text{MgO}$ ,  $\text{Al}_2\text{O}_3$ ,  $\text{K}_2\text{O}$ ,  $\text{CaO}$ ,  $\text{MnO}$ ,  $\text{BaO}$ ,  $\text{CuO}$ ,  $\text{P}_2\text{O}_5$ ,  $\text{CdO}$ ,  $\text{SnO}_2$ ,  $\text{As}_2\text{O}_3$ . The thermostatic analyses and dehydrochlorination test were performed in the DHC device at the Eskişehir Osmangazi University Molecular Spectroscopy and FT-IR laboratory. Surface heating test and thermal barrier tests were performed via Elimko 32 channel thermometer and with thermocouples by BR Dizayn Industrial Design Center Laboratory.

## 2.5 Thermostatic Analysis (DHC Test)

The ISO 182-2 standard was established to determine the thermal stability of vinyl chloride homopolymer and copolymer-based products and to determine the release tendencies of hydrogen chloride and other acidic components resulting from the oxidation of PVC while heat treatment. The stability time determined by the ISO 182-2 standard is measured by the time measured during the change in the initial PH value (6.00) and the test termination PH value (3.20) of the HCl gas released from the plastic at 200  $^{\circ}\text{C}$ . In this study, the plastic sheets obtained from the plasticization process are turned into 1  $\text{cm}^2$  square pieces and placed in the sample cell. 0.1 mol/L NaCl (125 ml) solution is added to the DHC test cell. High purity  $\text{N}_2$  gas is used as the conditioning gas to transmit the  $\text{H}^+$  and  $\text{Cl}^-$  ions that arise during the heating of the sample from the sample cup to the test cup. The gas flow rate is adjusted by a flow meter (120  $\text{cm}^3/\text{min}$ ). To adjust the DHC cell to the initial PH value (6.00), 0.1 mol/L NaOH solution and 0.1 mol/L HCl solution are used as PH stabilizers. The Dehydrochlorization test system is given in Figure 3.

## 2.6 Heat Barrier Test Unit

The plastic materials produced from plastic doughs containing new generation plastic additives were shaped with the help of a knife to frame the built-in hobs burners, placed between the built-in hobs surface and the burners. Then built-in hobs were mounted. Thermocouples connected to Elimko branded 32-channel T-type thermometer are placed on the surface, bottom plate, and inside of the built-in hob. Hence, the surface temperatures were thus transmitted to the digital thermometer.

The experiment was carried out in 3 phases. In the first phase, commercial gaskets were used and the furnace temperature values were obtained during heating and cooling. In the second phase, heating and cooling tests were carried out on plastic materials obtained with plastic doughs containing Mn (II) or Cu (II), respectively. Finally, the data obtained from the three tests were placed on top of each other and the heat barrier results were compared.

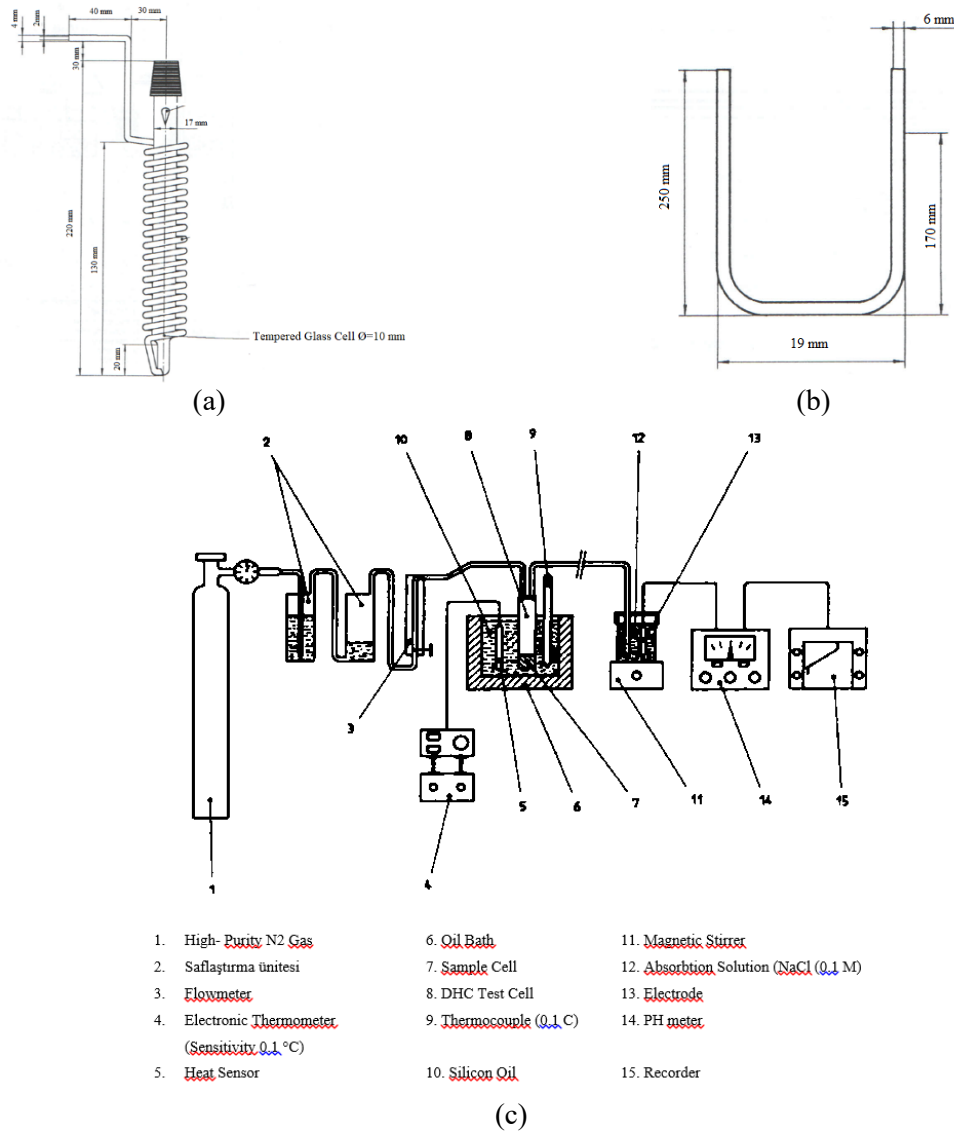


Figure 3. Thermostatic Analysis test unit: (a) Sample Cell, (b) U-type sample cell, (c) DHC test unit.

### 3. Results and Discussion

In this study,  $Mn(C_{18}H_{36}O_2)_2 \cdot (B_4O_7) \cdot 2H_2O$  (1),  $Cu(C_{18}H_{35}O_2)_2 \cdot (B_4O_7) \cdot H_2O$  (2) were synthesized as a new generation plastic additive and obtained as powder. The structural properties of the synthesized complexes were investigated by FT-IR and Raman spectroscopy, XRD diffraction, XRF spectroscopy, and gravimetric thermal analysis methods. Plastic blend was obtained by using synthesized new generation plastic additives. The obtained plastic blends were turned into plastic by plasticization method. The thermal stability of the plasticized materials was determined by thermostatic analysis. In addition, the thermal barrier behavior of the obtained plastic materials was examined and compared with the thermal barrier behavior of standard commercial gaskets.

#### 3.1 Structural Analyses

Vibration spectroscopy (FT-IR, Raman) analysis of the complexes was investigated based on the stearate and borate vibrational wavenumbers in the complexes. In addition, the metal oxide bond vibration wavenumbers of the synthesized complexes were compared with the metal-oxide bond vibration wavenumbers obtained from some studies in the literature [11, 12]. Infrared spectra of sodium stearate, sodium borate as ligands in this study are given in Figures 4 and FT-IR and Raman spectra of the complexes are given between Figures 5.

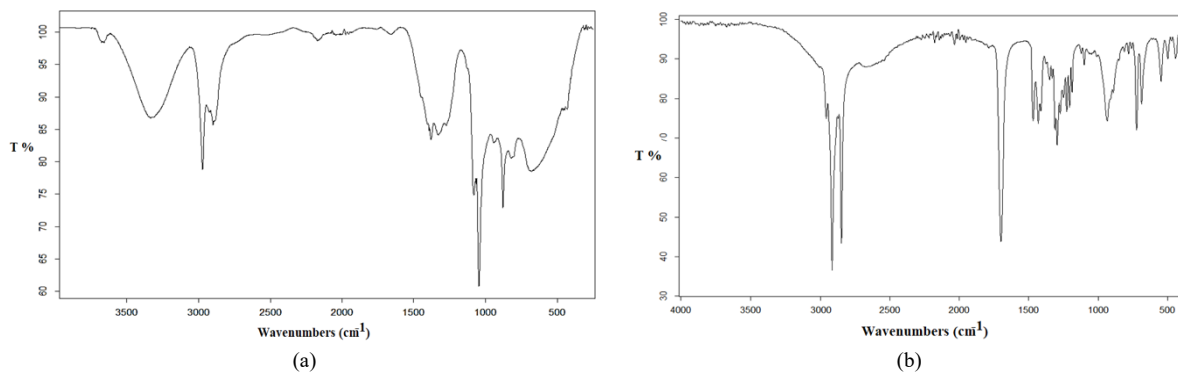


Figure 4. The infrared spectra of sodium tetraborate (a), sodium sterate (b)

As seen in Table 5,  $\nu(\text{OH})$  stretching and  $\nu(\text{H-O-H})$  bending vibration bands are observed in wave numbers of  $3405 \text{ cm}^{-1}$  and  $1652 \text{ cm}^{-1}$ , respectively [11]. For this region, vibration bands with wave numbers of  $1432 \text{ cm}^{-1}$ ,  $1344 \text{ cm}^{-1}$ , and  $1258 \text{ cm}^{-1}$  were determined as asymmetric stretch vibration bands of the B-O bond in  $\text{BO}_3$ . In the complexes, the borate ligand is expected to coordinate through the oxygen atoms. For this reason, a shift to the high-frequency region is expected for  $\nu(\text{B-O})$  stretching vibrations and  $\delta(\text{O-B-O})$  bending vibrations. For the sodium borate ligand,  $\nu(\text{B-O})$  stretching vibrations were recorded at  $1432 \text{ cm}^{-1}$ ,  $1344 \text{ cm}^{-1}$ , and  $1258 \text{ cm}^{-1}$ , respectively, while  $\delta(\text{O-B-O})$  were recorded at  $500 \text{ cm}^{-1}$  and  $454 \text{ cm}^{-1}$ .

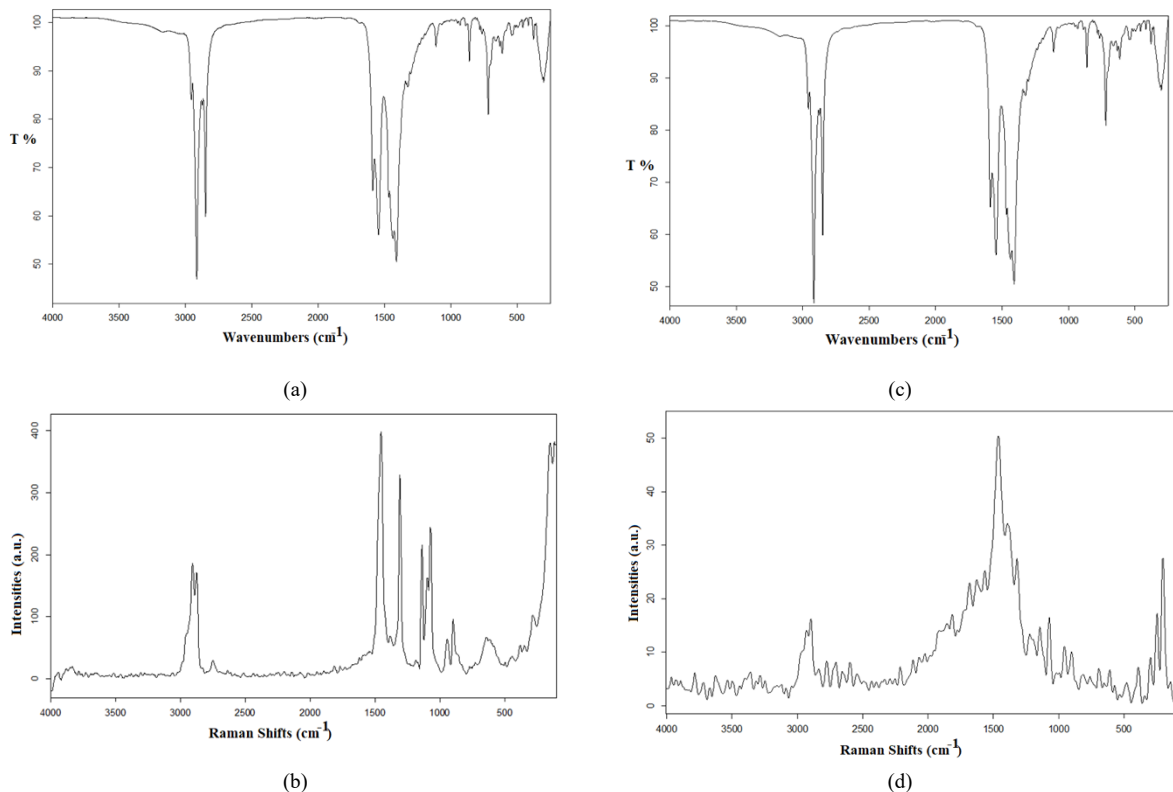


Figure 5. The FT-IR and Raman spectra of 1 (a,b), 2 (c,d).

The vibration bands at wave numbers  $1130 \text{ cm}^{-1}$  and  $1076 \text{ cm}^{-1}$  for sodium borax are due to the asymmetric stretching of the B-O bond in  $\text{BO}_4$  [11]. While this vibration band was observed at  $1159 \text{ cm}^{-1}$  and  $1087 \text{ cm}^{-1}$  wave numbers for the  $\text{Mn}(\text{B}_4\text{O}_7)_2 \cdot 2\text{H}_2\text{O}$  complex, it was observed at  $1176 \text{ cm}^{-1}$  and  $1109 \text{ cm}^{-1}$  wave numbers for the **1** complex.

Table 5. Borate anions wavenumbers in the complexes ( $\text{cm}^{-1}$ )

Assignments <sup>*a</sup>	Sodium Borate FT-IR <sup>a</sup>	Mn(B <sub>4</sub> O <sub>7</sub> ) <sub>2</sub> ·2H <sub>2</sub> O FT-IR	(1)		(2)	
			FT-IR	Raman	FT-IR	Raman
$\nu(\text{OH})$	3405 br	-	-	-	-	3490 vw
$\delta(\text{HOH})$	1652 m	-	1686 br	-	1698 br	1637 m
$\nu(\text{B-O})$ from $\text{BO}_3$	1432 s	1456 m	1435 s	1437 m	1438 br	1469 vs
$\nu(\text{B-O})$ from $\text{BO}_3$	1344 m	1405 m	1409 s	-	1416 vw	-
$\nu(\text{B-O})$ from $\text{BO}_3$	1258 w	1298 w	1320 w 1299 w	- 1304 m	1322 br 1302 vw	1315 s
$\nu_{\text{as}}(\text{B-O})$ from $\text{BO}_4$	1130 w	1159 vw	1112 w	1132 m	1113 vw	1135 m
$\nu_{\text{as}}(\text{B-O})$ from $\text{BO}_4$	1076 m	1087 w	1068 w	1065 w	1097 vw	1069 m
$\nu(\text{B-O})$ from $\text{BO}_4$	944 m	979 w	1006 vw	-	-	1021 w
$\nu(\text{B-O})$ from $\text{BO}_4$	826 s	862 m	861 w	-	861 m	873 sh
$\delta(\text{B-O})$ from $\text{BO}_3$	710 w	-	718 s 708 sh	716 vw	718 m 703 sh	716 sh
$\delta(\text{O-B-O})$	500 w	529 w	510 vw	-	532 vw	575 w 524 vw
$\delta(\text{O-B-O})$	454 m	482 w	489 vw	-	493 vw	485 m

\* $\nu$ : stretching;  $\delta$ : bending, s: symmetric as: asymmetric, s: strong, m: medium; w: weak; sh: shoulder <sup>a</sup>[11]

It is seen that the B-O asymmetric stretching vibrations observed in the complexes are shifted to higher frequencies than sodium borate. Similarly, symmetric stretching bands of B-O in  $\text{BO}_3$  and  $\text{BO}_4$  were observed at wave numbers of  $944 \text{ cm}^{-1}$  and  $826 \text{ cm}^{-1}$ . Planar bending of B-O in  $\text{BO}_3$  is observed at a wave number of  $710 \text{ cm}^{-1}$  [11]. These vibration bands were observed in the **1** complex at wave numbers of  $979 \text{ cm}^{-1}$  and  $862 \text{ cm}^{-1}$ . The symmetrical stretching and out-of-plane bending vibrations of the B-O bond were observed at higher frequencies in the complexes than in the sodium borate crystal. Finally, the vibrational bands at  $454 \text{ cm}^{-1}$  and  $500 \text{ cm}^{-1}$  are due to  $\delta_{\text{ring}}(\text{O-B-O})$  in the structure [11]. Wave numbers of  $482 \text{ cm}^{-1}$  and  $529 \text{ cm}^{-1}$  were observed for the  $\delta_{\text{ring}}(\text{O-B-O})$  for **2** complexes. It was determined that the  $\delta_{\text{ring}}(\text{O-B-O})$  deformation vibration shifted to higher frequency values from sodium borate.

The characteristic vibrational bands for stearic acid are listed in Table 6. Characteristic vibration bands are asymmetric and symmetrical carbonyl group vibrations  $\nu(\text{COO}^-)$ ,  $\nu(\text{CH}_x)$  stretching are asymmetric and symmetric stretching vibrations from ethylene and methylene groups [13-17]. According to the literature, for the stearate vibration bands, the vibration bands at  $2963 \text{ cm}^{-1}$  and  $2877 \text{ cm}^{-1}$  in the C-H stretching region were observed as asymmetric and symmetric stretching vibration bands of the methyl group, respectively. In addition,  $\nu_{\text{as}}(\text{CH}_3)$  and  $\nu_{\text{s}}(\text{CH}_3)$  vibrations of the methylene group were recorded at wave numbers of  $2917 \text{ cm}^{-1}$  and  $2849 \text{ cm}^{-1}$ , respectively [13-17].

The coordination point for the stearate anion is the carbonyl group via electronegative oxygen atoms. For this reason, the study is focused on the stress and bending vibration wave numbers of the carbonyl group. While the  $\nu(\text{C=O})$  strain vibration was observed at  $1697 \text{ cm}^{-1}$  in stearic acid, this vibrational band is recorded at  $1689 \text{ cm}^{-1}$  for Complex **1** and  $1676 \text{ cm}^{-1}$  for Complex **2**. It was observed that the C=O stretching vibration mode shifted to the low-frequency region in the complexes. However,  $\nu(\text{COO}^-)$  stretching vibrations were observed at  $1518 \text{ cm}^{-1}$  in stearic acid, while  $1587 \text{ cm}^{-1}$  for complex **1** and complex **2** were observed. It was determined that the stress vibration frequency  $\nu(\text{COO}^-)$  shifted to the high-frequency region. Thus, it is thought that coordination is provided through oxygen atoms.

Table 6. Vibration wavenumbers of stearic acid in complexes (cm<sup>-1</sup>)

Assignments *, a,b,c,d,e,f,g	Stearic Acid			(1)		(2)	
	FT-IR	FT-IR	Raman	FT-IR	Raman	FT-IR	Raman
v <sub>as</sub> (CH <sub>3</sub> )	2964	-	2933 sh	3171 vw	3157 vw		
v <sub>as</sub> (CH <sub>3</sub> )	2954	2956 w	-	2957m	2953 sh		
v <sub>s</sub> (CH <sub>3</sub> )	2937	-	-	-	2926 m		
v <sub>as</sub> (CH <sub>2</sub> )	2918	2915 vs	-	2916 vs	-		
v <sub>s</sub> (CH <sub>3</sub> )	2870	2875 m	2882 w	2873 m	2894 s		
v <sub>s</sub> (CH <sub>2</sub> )	2850	2849 vs	2848 w	2850 vs	2828 m		
v(C=O)	1697	1689 w	-	-	1676 m		
v <sub>as</sub> (COO <sup>-</sup> )	1518	1587 vs	-	1587 vw	-		
δ <sub>sc</sub> (CH <sub>2</sub> )	1471	1544 vs	-	1561 sh	1566 m		
δ <sub>sc</sub> (CH <sub>2</sub> )	1470	1467 m	-	-	-		
δ <sub>sc</sub> (CH <sub>2</sub> )	1464	-	-	-	-		
δ <sub>sc</sub> (CH <sub>2</sub> )	1458	-	-	-	-		
v(C-O)+ v(O-H)	1437	1440 sh	-	-	-		
v(C-O)+ v(O-H)	1431	-	-	-	-		
v <sub>s</sub> (COO <sup>-</sup> )	1419	1417 sh	-	1410 m	-		
δ <sub>sc</sub> (CH <sub>2</sub> )	1416	-	-	-	-		
δ <sub>w</sub> (CH <sub>2</sub> )	1369	1384 sh	-	1376 sh	-		
δ <sub>w</sub> (CH <sub>2</sub> )	1357	1377 sh	-	-	1386 s		
δ <sub>w</sub> (CH <sub>2</sub> ) + δ <sub>tw</sub> (CH <sub>2</sub> )	1350	-	-	-	-		
δ <sub>w</sub> (CH <sub>2</sub> )	1348	1352 vw	-	1353 vw	-		
δ <sub>w</sub> (CH <sub>2</sub> ) + δ <sub>tw</sub> (CH <sub>2</sub> ) + δ <sub>rock</sub> (CH <sub>2</sub> )	1333	1335 vw	-	1335 vw	-		
δ <sub>w</sub> (CH <sub>2</sub> ) + δ <sub>tw</sub> (CH <sub>2</sub> ) + δ <sub>rock</sub> (CH <sub>2</sub> )	1318	1321 w	-	-	1315 s		
δ <sub>w</sub> (CH <sub>2</sub> ) + δ <sub>tw</sub> (CH <sub>2</sub> ) + δ <sub>rock</sub> (CH <sub>2</sub> )	1300	1303 vw	-	-	-		
δ <sub>w</sub> (CH <sub>2</sub> ) + δ <sub>tw</sub> (CH <sub>2</sub> ) + δ <sub>rock</sub> (CH <sub>2</sub> )	1281	1289 sh	-	-	1292 sh		
δ <sub>w</sub> (CH <sub>2</sub> ) + δ <sub>tw</sub> (CH <sub>2</sub> ) + δ <sub>rock</sub> (CH <sub>2</sub> )	1263	1277 vw	-	-	1272 sh		
δ <sub>w</sub> (CH <sub>2</sub> ) + δ <sub>tw</sub> (CH <sub>2</sub> ) + δ <sub>rock</sub> (CH <sub>2</sub> )	1244	1257 vw	-	1258 vw	-		
δ <sub>w</sub> (CH <sub>2</sub> ) + δ <sub>tw</sub> (CH <sub>2</sub> ) + δ <sub>rock</sub> (CH <sub>2</sub> )	1225	1233 vw	-	1235 vw	1225 w		
δ <sub>w</sub> (CH <sub>2</sub> ) + δ <sub>tw</sub> (CH <sub>2</sub> ) + δ <sub>rock</sub> (CH <sub>2</sub> )	1206	1213 w	-	1210 br	1219 m		
δ <sub>w</sub> (CH <sub>2</sub> ) + δ <sub>tw</sub> (CH <sub>2</sub> ) + δ <sub>rock</sub> (CH <sub>2</sub> )	1187	1191 vw	-	1190 sh	1194 sh		
δ <sub>w</sub> (CH <sub>2</sub> ) + δ <sub>tw</sub> (CH <sub>2</sub> ) + δ <sub>rock</sub> (CH <sub>2</sub> )	1150	1168 sh	-	-	-		

v: stretching, δ: bending, δ<sub>w</sub>: wagging, δ<sub>tw</sub>: twisting, δ<sub>sc</sub>: scissoring, s: symmetric, as: asymmetric

<sup>a</sup>[17](Lee ve Kim 1998), <sup>b</sup>[18](Hostetler, Stokes vd 1996), <sup>c</sup>[19](Snyder 1967), <sup>d</sup>[14](Snyder, Strauss vd 1982), <sup>e</sup>[20](Allara ve Nuzzo 1985), <sup>f</sup>[15](Rabolt, Burns vd 1983), <sup>g</sup>[13](Snyder ve Schachtschneider 1963)

PXRD diffraction patterns as new generation plastic additives of the complexes are given in Figure 6. The PXRD diffraction patterns of the complexes were clarified with the Match 3.0 Rietveld program [21]. Structure studies by comparing the PXRD diffraction patterns of the complexes with the matching structures from the literature. In addition, data from XRD diffraction patterns are listed in Table 7 by comparison with metal-oxide vibrational wavenumbers observed by vibrational spectroscopy.

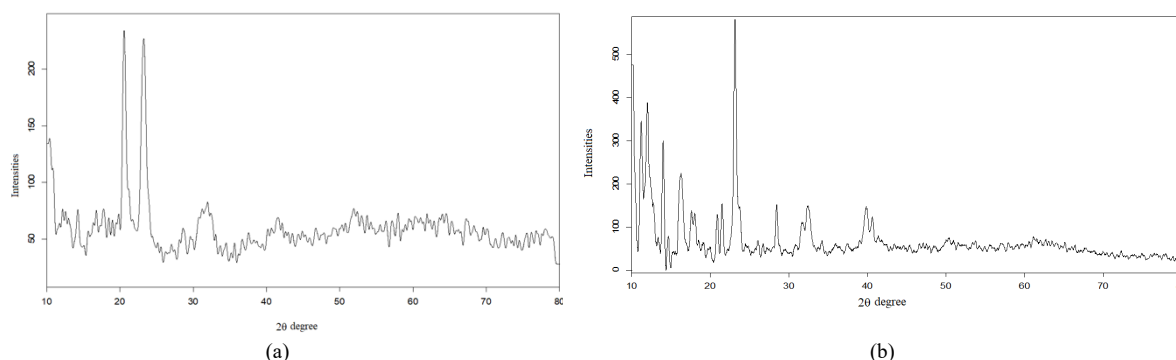


Figure 6. The XRD diffraction pattern for 1 (a) and (2) (b)

By Rietvielt analysis [26], the PXRD diffraction pattern of **1** was determined to match the powder pattern of sodium tetraboratedecahydrate molecule [12] with monoclinic a= 11.8843 Å b= 10.6026 Å c= 12.2111 Å β= 106,790 ° unit cell parameters with 47.5% probability [12]. Additionally, the PXRD diffraction pattern of the Complex was found to match with the monoclinic C<sub>10</sub>Mn<sub>2</sub>O<sub>10</sub> structure with a

probability of 30.5%, with a unit cell  $a= 14.1257 \text{ \AA}$ ,  $b= 6.8799 \text{ \AA}$ ,  $c= 14.3121 \text{ \AA}$ ,  $\beta= 105.07$  [22]. Moreover, the PXRD diffraction pattern for 1.1 was found to be compatible with  $\text{Mn}_2\text{O}_3$  with a 22% probability orthorhombic cell  $a= 9.4118 \text{ \AA}$   $b= 9.4177 \text{ \AA}$   $c= 9.4233 \text{ \AA}$  [23].

**Table 7.** XRD powder diffraction pattern matching and vibrational wavenumbers corresponding to metal oxide bonds in complexes ( $\text{cm}^{-1}$ )

Complex	Molecular Formula	Matched structure of PXRD diffraction pattern for the complexes*	Vibrational Spectroscopy (Metal-Oxide wavenumbers) $\text{cm}^{-1}$			
			Assignments*	Wavenumbers ( $\text{cm}^{-1}$ )		
1	$\text{Mn}(\text{C}_{18}\text{H}_{36}\text{O}_2)_2 \cdot (\text{B}_4\text{O}_7) \cdot 2\text{H}_2\text{O}$	<sup>a</sup> $\text{Na}_2\text{B}_4\text{O}_7$ <sup>b</sup> $\text{C}_{10}\text{Mn}_2\text{O}_{10}$ <sup>c</sup> $\text{Mn}_2\text{O}_3$	Assignments*	Wavenumbers ( $\text{cm}^{-1}$ )		
				<sup>d</sup> IR	IR	Raman
			$\beta\text{-MnO}_2$	618	611	619
			$\beta\text{-MnO}_2$	545	-	520
			$\beta\text{-MnO}_2$	387	-	383
2	$\text{Cu}(\text{C}_{18}\text{H}_{35}\text{O}_2)_2 \cdot (\text{B}_4\text{O}_7) \cdot \text{H}_2\text{O}$	$\text{Cu}(\text{CNB}_4\text{O}_7)_4$ <sup>a</sup> $\text{Na}_2\text{B}_4\text{O}_7$	Assignments*	Wavenumbers ( $\text{cm}^{-1}$ )		
				IR	IR	Raman
			$\nu(\text{Cu-O})$	470	-	487
			$\nu(\text{Cu-O})$	440	438	-

\*<sup>a</sup>[12](Gainsford et al, 2008); <sup>b</sup>[22] (Louis et al, 1967) <sup>c</sup>[23] (Norrestam et al,1967); <sup>d</sup>[24](Julien et al. , 2004) <sup>e</sup>[25] (Hibble et al, 2002)

For Complex 2, The PXRD diffraction pattern of the complex was matched by Rietveld analyses via the Match 3 program with copper tetracyano borate with a cubic  $a=5.4314 \text{ \AA}$  unit cell with a ratio of 58.2%. According to this result, it is seen that the borate  $(\text{B}_4\text{O}_7)^{2-}$  anion binds to the Cu(II) atom from the oxygen end [27]. In addition, the PXRD diffraction pattern of the Complex was matched with a monoclinic  $a= 11.8900 \text{ \AA}$   $b= 10.7400 \text{ \AA}$   $c= 12.1900 \text{ \AA}$   $\beta= 106,580^\circ$  unit cell with a ratio of 41.8% [27]. Thus, the presence of borate anion in the formula proposed according to the results of the elemental analysis was also supported by PXRD powder diffraction.

The XRF data of the complexes were analyzed based on the intensity, mass ratio and v/o ratio. XRF data analysis results are given in Table 8 and Table 9, and the data are compared graphically in Figure 5 and Figure 6. The molecular formula of complex 1 was determined as  $\text{Mn}(\text{C}_{18}\text{H}_{36}\text{O}_2)_2 \cdot (\text{B}_4\text{O}_7) \cdot 2\text{H}_2\text{O}$  by elemental analysis method. It is found as 87.46% probability that the complex has Mn-K $\alpha$  characteristic layer in XRF data. It is thought that Na-K $\alpha$  (4.47%) sodium oxides determined in the structure come from  $\text{Na}_2\text{B}_4\text{O}_7 \cdot 10\text{H}_2\text{O}$  or  $\text{NaC}_{18}\text{H}_{36}\text{O}_2$  during the complex formation. The trace amount of determined Cl ion is thought to be caused by the conversion of  $\text{MnCl}_2$  metal salt into  $\text{Mn}^{+2}$  and  $2\text{Cl}^-$  ions during the formation of the complex and forming as a salt solution according to the reaction with the  $\text{N}^+$  ions from sodium borate and sodium stearate. Trace amounts of aluminum and silicon oxide were observed in the structure. It can be said that the other metal oxides seen are due to the impurity of the metal salt.

Table 8. XRF data analyses for Complex 1

Element	Compound	Ratio	w/o normal	% Mass	Source Limit
Na-K $\alpha$	Na <sub>2</sub> O	0,0668	0,5809	4,47%	1,06331
Mg-K $\alpha$	MgO	0,0116	0,0332	0,00%	0,50853
Al-K $\alpha$	Al <sub>2</sub> O <sub>3</sub>	0,7273	0,4938	3,40%	0,43233
Si-K $\alpha$	SiO <sub>2</sub>	0,5893	0,3993	3,08%	0,15375
Cl-K $\alpha$	Cl	0,3428	0,1167	0,90%	0,17878
K-K $\alpha$	K <sub>2</sub> O	0,4255	0,397	0,31%	0,08122
Ca-K $\alpha$	CaO	0,5628	0,0518	0,40%	0,11842
Mn-K $\alpha$	MnO	164,2788	11,3664	87,46%	0,14380
Fe-K $\alpha$	Fe <sub>2</sub> O <sub>3</sub>	1,6488	0	0,00%	0,15810

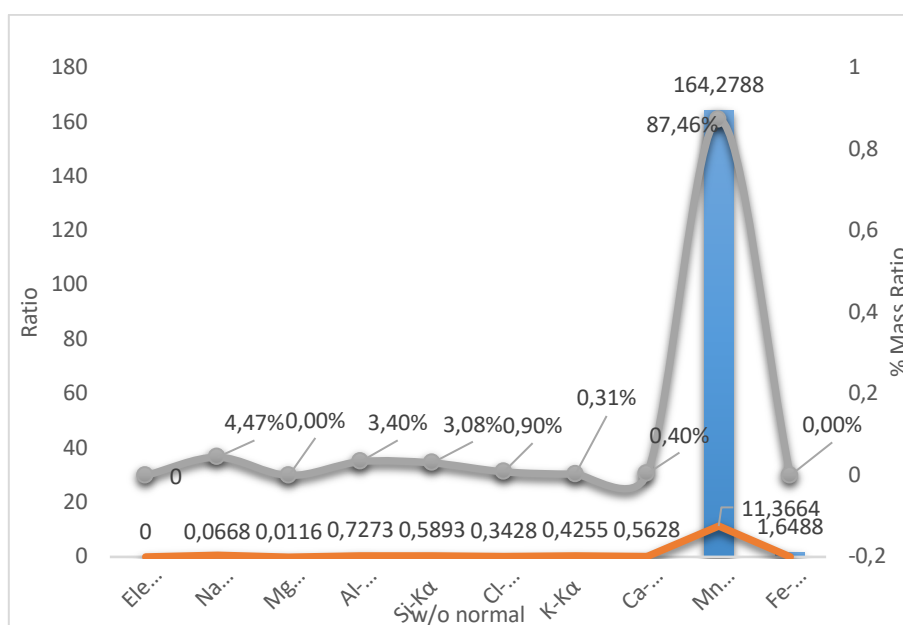


Figure 7. Graphical demonstration of obtained XRF data for Complex 1

Table 9. XRF data analyses for Complex 2

Element	Compound	Ratio	w/o normal	% Mass	Source Limit
Na-K $\alpha$	Na <sub>2</sub> O	0,1306	1,1371	6,85%	1,15612
Mg-K $\alpha$	MgO	0,0215	0,067	0,00%	0,45415
Si-K $\alpha$	SiO <sub>2</sub>	0,3641	0,2681	1,61%	0,08242
P-K $\alpha$	P <sub>2</sub> O <sub>5</sub>	0,0966	0,0223	0,13%	0,05603
Cl-K $\alpha$	Cl	0,5121	0,1915	1,15%	0,14900
Ca-K $\alpha$	CaO	0,3963	0,0492	0,30%	0,09397
Fe-K $\alpha$	Fe <sub>2</sub> O <sub>3</sub>	1,687	0,0679	0,41%	0,07434
Cu-K $\alpha$	CuO	669,8581	14,391	86,64%	0,76100
Ba-K $\alpha$	BaO	2,9356	0,4167	2,51%	0,92850

Similarly, The closed formula of complex 2 was determined as  $\text{Cu}(\text{C}_{18}\text{H}_{35}\text{O}_2)_2 \cdot (\text{B}_4\text{O}_7) \cdot \text{H}_2\text{O}$  by elemental analysis methods. It is found as 86.64% probability that the complex has Cu-K $\alpha$  characteristic layer in XRF data. It is thought that Na-K $\alpha$  (6.85%) sodium oxides determined in the structure come from  $\text{Na}_2\text{B}_4\text{O}_7 \cdot 10\text{H}_2\text{O}$  or  $\text{NaC}_{18}\text{H}_{36}\text{O}_2$  during the formation of the complex. The trace amount of Cl ion is thought to be caused by the decomposition of the  $\text{CuCl}_2$  metal salt into  $\text{Cu}^{+2}$  and  $2\text{Cl}^-$  ions during the formation of the complex, and the formation of a salt solution according to the reaction with the  $\text{N}^+$  ions from sodium borate and sodium stearate. Trace amounts of iron, silicon, phosphate, and barium oxide were observed in the structure. It can be said that the other metal oxides seen are due to the impurity of the metal salt.

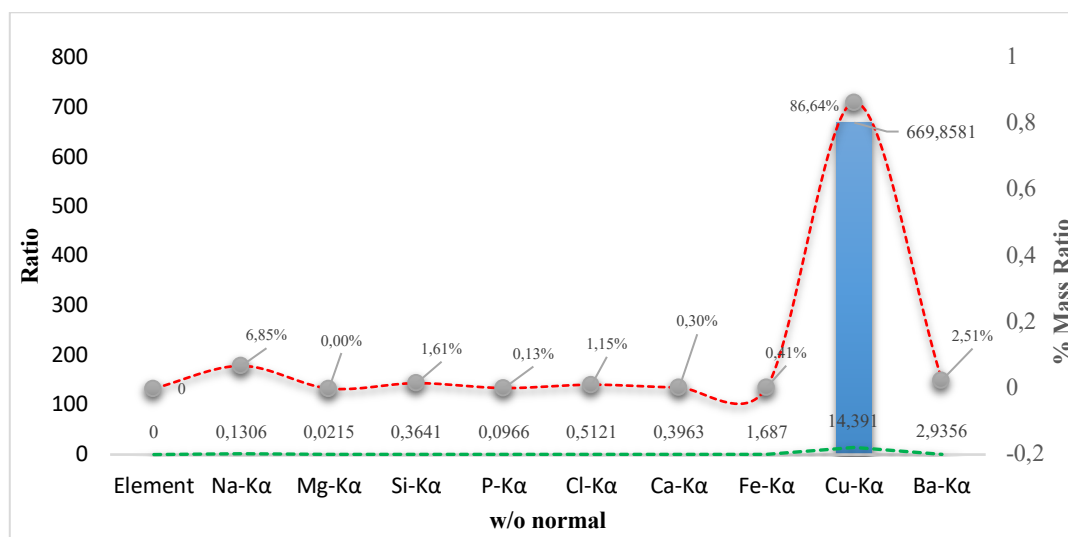


Figure 8. Graphical demonstration of obtained XRF data for Complex 2

### 3.2 Thermal stability and Thermal Barrier Analyses

The thermostatic analysis diagram of the new generation plastic additives obtained from the metal complexes of stearate and borate ligands obtained with Mn(II) and Cu(II) atoms is given in Figure 9. For the complexes,  $\text{Mn}(\text{C}_{18}\text{H}_{36}\text{O}_2)_2 \cdot (\text{B}_4\text{O}_7) \cdot 2\text{H}_2\text{O}$  and  $\text{Cu}(\text{C}_{18}\text{H}_{35}\text{O}_2)_2 \cdot (\text{B}_4\text{O}_7) \cdot \text{H}_2\text{O}$  scavenged. It is seen that the  $\text{H}^+$  and  $\text{Cl}^-$  ions formed by the thermal decomposition of PVC were scavenged till 65 minutes for 1 complex and 57 minutes for 2 complex. Sodium stearate and its derivatives have high thermal stability and are used in industry as a fire extinguisher and acid absorber material. Therefore, sodium stearate was preferred, considering both its resistance in acidic environments and its thermal stability. for both complexes at the 200 C temperature, a sudden increase occurs in the pH value of the plastic dough, which receives heat, and in this way, the acidic environment is quickly neutralized by the thermal degradation of PVC. Considering these results, it is suggested that a plastic additive with high thermal and UV resistance may be one of the basic building blocks. In addition, it was determined that complexes containing Mn(II) were more thermally stable, while complexes containing Cu(II) acted as stronger HCl scavenger material.

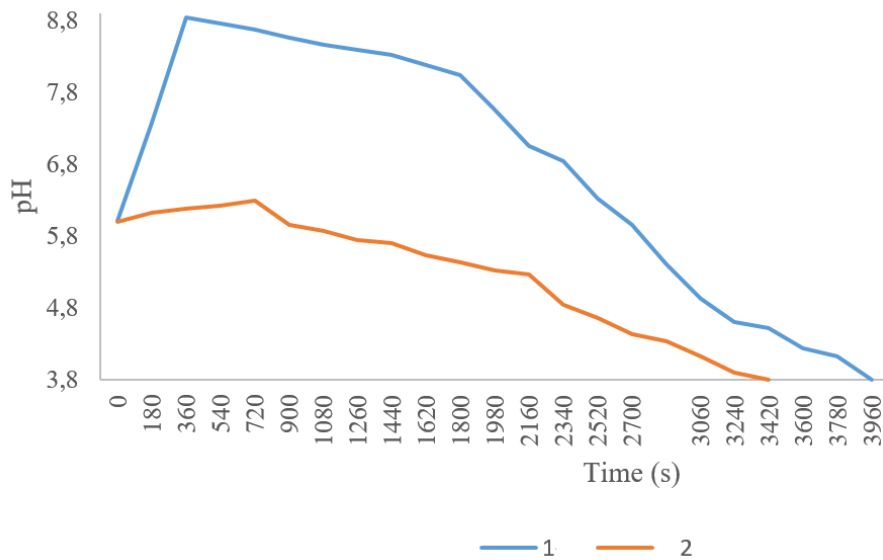


Figure 9. Thermostatic stability analysis of PVC dough containing New Generation Plastic additives

Obtained Plastic dough from new generation plastic additives is plasticized and made into gaskets. The gaskets are mounted between burners and the bottom of the built-in cooker surface. In this context, 3 tests were carried out. The first test concerns the testing of commercially used gaskets. The second test is about testing plastic materials containing complex 1, and the third test is about testing plastic materials containing complex 2. The test start temperature was set to 24 °C. Thermocouples are connected on three different hob surfaces containing three different gasket types and the data is connected to Elimko 32T digital thermometer with its probes. The tests were started simultaneously for three different built-in hobs by boiling 2.5 liters of water in three different built-in hobs. Thermal barrier tests for three different built-in cookers were carried out for 45 minutes. The tests were completed after 45 minutes. The variation of surface temperatures during the test is given in Figure 10.

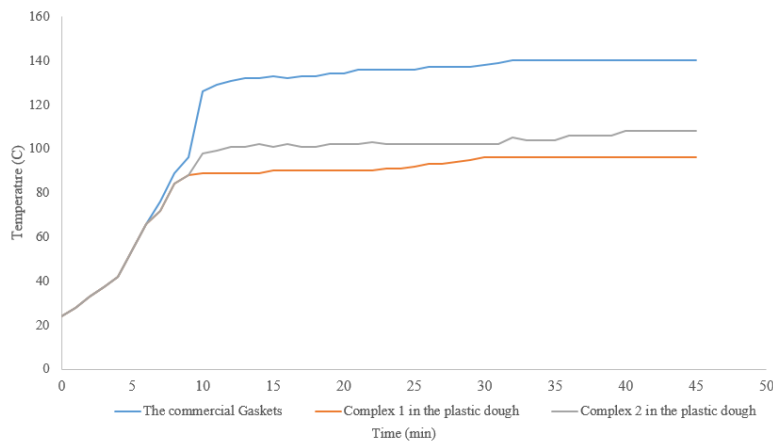


Figure 10. Thermal Barrier analysis of PVC dough containing New Generation Plastic additives

The most important reason for the surface heating of a built-in hob is the surface heating of the flame reflected from the bottom of the pans and pots on the built-in hob grids. In particular, reasons such as yellowing of the stainless steel surface and glass bursts are due to the heat dissipation not being correct. During the test, it was determined that the surface temperature reached 140 °C for commercially used gaskets, but the gaskets obtained with plastic doughs containing new generation plastic additives heated the surface less.

#### 4. Conclusion

In this study, Mn(II) and Cu(II) metal complexes of borate and stearate ligands were synthesized. The closed formulas of the synthesized metal complexes were determined by elemental analysis methods and supported by thermogravimetric analysis methods (TG-DTA and DTG). Structural analyzes of the obtained metal complexes were clarified by vibration spectroscopy (FT-IR and Raman), XRD spectroscopy and XRF spectroscopy methods, respectively.

The data obtained from the FT-IR and Raman spectra of the complexes were compared with the Stearic acid and Sodium borate vibrational wave numbers in the literature. The shifts in the vibrational wavenumbers obtained that the complexes coordinate with the oxygen donor atoms and that these components take place in the structures. The existence of metal oxide bonds in the complexes has been explained by vibration spectroscopy and the presence of metal-oxide bonds has been supported by XRD spectroscopy methods and XRF methods.

The obtained metal complexes were blended with the components of standard plastic dough according to their mass percent composition, and they were turned into plastic by gelling.

The thermal stability of the plasticized materials was investigated by the thermostatic analysis method described in the ISO 182-2 standard. It has been determined that the plastic materials obtained with the synthesized complexes are HCl scavenger materials. According to the test results, it was determined that the complex containing Mn(II) was more stable than the complex containing Cu(II).

Plastic materials obtained with metal complexes were located between the surface of the built-in hob and the burners, and the temperature changes of the built-in hob surface were examined according to the EN 30-1-1+A3:2014 standard. It has been determined that gaskets obtained from plastic dough containing new generation plastic additives have higher thermal barrier capacity than commercial gaskets.

This study can be considered as an initial study. In particular, while obtaining plastic material in this study, thermal barrier capacities of plastic additives can be improved by changing the type of plastic raw material, its hardness or ratio, filler type or ratio, or the type or ratio of other plastic additives. Thus, the usage areas of plastic will be extended.

#### ACKNOWLEDGEMENTS

The author highly thankful to the Eskişehir Osmangazi University, Scientific research Unit (Project No. 2017-1588). Additionally, thank you to Prof.Dr. Güneş Süheyla Kürkçüoğlu due to provide laboratory facilities for synthesis and obtaining spectroscopic data.

#### REFERENCES

1. Kavlak İ, Kürkçüoğlu GS, and Şahin O. Investigation of structural analysis and thermostatic properties of thermal and UV stabilizer as organometallic Sn (II), Cu (II) and Cd (II) barbiturate complexes. *J. Mol. Struct.* 2019; 1184: p. 418-426.
2. Bhaskar K, Jayabalakrishnan D, Kumar MV, Sendilvelan S, and Prabhakar M. Analysis on mechanical properties of wood plastic composite. *Materials Today: Proceedings 2021*; 45: p. 5886-5891.
3. Fisch M and Bacaloglu R. Study of additive compatibility with poly (vinyl chloride)(PVC). 2: Dynamic mechanical analysis of PVC lubrication by stearic acid and its derivatives. *J. Vinyl Addit. Technol.* 1998; 4(1): p. 4-11.
4. Reedy ME and Dudek S. New Polymeric Foam Technologies. In: *Foaming Conference, RAPRA, Frankfurt, Germany*; 2001.
5. Atakul S and Balköse D. Nano-Zinc Borates as Polyvinyl Chloride Thermal Stabilizers. In *Engineering Technology and Industrial Chemistry with Applications: Apple Academic Press*, 2018.
6. Santamaria E, Edge M, Allen N, Harvey H, Mellor M, and Orchison J. New insights into the degradation mechanism of poly (vinyl chloride), Part (III): Implementation of new

- costabilizers—Towards heavy metal free systems (HMFS). *J. Appl. Polym. Sci.* 2005; 96(1): p. 122-143.
7. Li S and Yao Y. Effect of thermal stabilizers composed of zinc barbiturate and calcium stearate for rigid poly (vinyl chloride). *Polym. Degrad. Stab.* 2011; 96(4): p. 637-641.
  8. Xu X, Chen S, Tang W, Qu Y, and Wang X. Investigation of basic zinc cyanurate as a novel thermal stabilizer for poly (vinyl chloride) and its synergistic effect with calcium stearate. *Polym. Degrad. Stab.* 2014; 99: p. 211-218.
  9. El-Khatib A, Fawzy M, and Abou Taleb W. Attenuation of D+ T neutrons in borated low density polyethylene. *Mater. Lett.* 1996; 26(1-2): p. 59-63.
  10. Wiles Dt and Young R. A new computer program for Rietveld analysis of X-ray powder diffraction patterns. *J. Appl. Crystallogr.* 1981; 14(2): p. 149-151.
  11. Goel N, Sinha N, and Kumar B. Growth and properties of sodium tetraborate decahydrate single crystals. *Mater. Res. Bull.* 2013; 48(4): p. 1632-1636.
  12. Gainsford GJ, Kemmitt T, and Higham C. Redetermination of the borax structure from laboratory X-ray data at 145 K. *Acta Crystallographica Section E: Structure Reports Online* 2008; 64(5): p. i24-i25.
  13. Snyder R and Schachtschneider J. Vibrational analysis of the n-paraffins—I: Assignments of infrared bands in the spectra of C<sub>3</sub>H<sub>8</sub> through n-C<sub>19</sub>H<sub>40</sub>. *Spectrochim. Acta* 1963; 19(1): p. 85-116.
  14. Snyder R, Strauss H, and Elliger C. Carbon-hydrogen stretching modes and the structure of n-alkyl chains. 1. Long, disordered chains. *J. Phys. Chem. A* 1982; 86(26): p. 5145-5150.
  15. Rabolt J, Burns F, Schlotter N, and Swalen J. Anisotropic orientation in molecular monolayers by infrared spectroscopy. *J. Chem. Phys.* 1983; 78(2): p. 946-952.
  16. Schlotter N, Porter MD, Bright T, and Allara DL. Formation and structure of a spontaneously adsorbed monolayer of arachidic on silver. *Chem. Phys. Lett.* 1986; 132(1): p. 93-98.
  17. Lee SJ and Kim K. Diffuse reflectance infrared spectra of stearic acid self-assembled on fine silver particles. *Vib. Spectrosc.* 1998; 18(2): p. 187-201.
  18. Hostetler MJ, Green SJ, Stokes JJ, and Murray RW. Monolayers in three dimensions: synthesis and electrochemistry of  $\omega$ -functionalized alkanethiolate-stabilized gold cluster compounds. *Journal of the American Chemical Society* 1996; 118(17): p. 4212-4213.
  19. Snyder RG. Vibrational study of the chain conformation of the liquid n - paraffins and molten polyethylene. *The Journal of Chemical Physics* 1967; 47(4): p. 1316-1360.
  20. Allara DL and Nuzzo RG. Spontaneously organized molecular assemblies. 2. Quantitative infrared spectroscopic determination of equilibrium structures of solution-adsorbed n-alkanoic acids on an oxidized aluminum surface. *Langmuir* 1985; 1(1): p. 52-66.
  21. Rodríguez-Carvajal J. Recent advances in magnetic structure determination by neutron powder diffraction. *Phys. B: Condens. Matter* 1993; 192(1-2): p. 55-69.
  22. Louis-Jean J, George J, and Poineau F. From ammonium Hexahalorhenates (IV) to nanocrystalline rhenium metal: A combined thermal, diffraction and microscopic analysis. *IJRMHM* 2022; 105: p. 105840.
  23. Norrestam R. a-Manganese (III) oxide—A C-type sesquioxide of orthorhombic symmetry. *Acta Chem. Scand.* 1967; 21: p. 2871-2884.
  24. Julien C, Massot M, and Poinignon C. Lattice vibrations of manganese oxides: Part I. Periodic structures. *Spectrochim. Acta A Mol. Biomol. Spectrosc.* 2004; 60(3): p. 689-700.
  25. Hibble SJ, Cheyne SM, Hannon AC, and Eversfield SG. CuCN: a polymorphic material. Structure of one form determined from total neutron diffraction. *Inorg. Chem.* 2002; 41(20): p. 4990-4992.
  26. Rietveld HM. A profile refinement method for nuclear and magnetic structures. *J. Appl. Crystallogr.* 1969; 2(2): p. 65-71.
  27. Font Tullot JM. El borax como estructura cristalina en cadenas. *Estud. Geol.* 1947; 7: p. 13-20.